

Available online at [www.sciencedirect.com](http://www.sciencedirect.com)

Chemical Engineering Research and Design

journal homepage: [www.elsevier.com/locate/cherd](http://www.elsevier.com/locate/cherd)

IChemE



# In-line monitoring of mixing performance for smart processes in tubular reactors

Zechen Yao<sup>1</sup>, Federico Alberini\*, Giuseppina Montante, Alessandro Paglianti

Department of Industrial Chemistry 'Toso Montanari', University of Bologna, via Terracini 34, 40131 Bologna, Italy

## ARTICLE INFO

### Article history:

Received 5 December 2022

Received in revised form 2 May 2023

Accepted 5 May 2023

Available online 8 May 2023

### Keywords:

Continuous process

Electrical resistance tomography

Pressure drop

Kenics static mixer

Tubular reactors

## ABSTRACT

This work is focused on the experimental analysis of the fluid dynamics characteristics of a tubular reactor equipped with Kenics static mixers working under turbulent flow conditions, with the specific aim of demonstrating the advantages of in-line monitoring tools for continuous process applications. Electrical Resistance Tomography, pressure transducers and Particle Image Velocimetry are employed to evaluate the mixing performance, the pressure drop and the flow field, respectively, considering the standard configuration of the mixers, consisting in mixing elements with alternating orientation, a single mixing element or multiple elements with the same orientation. The applicability of Electrical Resistance Tomography for offering insight into continuous reactors is assessed and the potential of monitoring the mixing performance inside the static mixers is shown. The experimental data suggest that alternatives to the standard element configurations might be adopted for optimizing the fluid mixing process, taking into account the mixing performances and the pressure drop, for which a novel correlation based on distributed and concentrated contributions is proposed.

© 2023 The Authors. Published by Elsevier Ltd on behalf of Institution of Chemical Engineers.

## 1. Introduction

In the European Roadmap of process intensification (PI), PI is defined as a set of innovative principles applied in process and equipment design, which can bring significant benefits in terms of process and chain efficiency, lower capital and operating expenses, higher quality of products, less wastes and improved process safety (Dimian et al., 2014).

Continuous processing, for many liquid product productions, which includes for instance fast moving consumer goods (FMCG), chemicals, pharmaceutical (Rohkohl et al., 2022), is the most viable manufacturing approach. This is mainly driven by better energy efficiency, enhanced process flexibility and high throughput.

When dealing with the design of continuous stirred tank reactors, we generally tend to assume that concentration and

temperature of reaction materials in the reactor are uniform, which is essentially the result of a perfectly-mixed flow model. This uniformity is due to vigorous agitation. However, in real system it is known that under agitation, some fluid parcels that enters the reactor may escape through the exit immediately, which results in very short residence times; while some other parcels may be agitated back from the exit, which makes their residence times extremely long. Hence, residence times distribution in real continuous tank reactors are very uneven (Li, 2017). The plug flow reactor is the second-most primary ideal reactor, but, as in continuous stirred tanks, deviations from the ideal model occur in practice and the control of the degree of irregularities is critical (Baronti et al., 2022). Often, to enhance the mixing inside continuous reactors and to shorten the length to achieve good mixing, static mixers are used.

Static or motionless mixers consist of a series of identical inserts or elements, arranged in a structured configuration, which can be installed in pipes, channels, columns or reactors (Valdés et al., 2022). These inserts are added to promote a chaotic mixing behaviour by dividing and redistributing the flow streamlines sequentially, following

\* Corresponding author.

E-mail address: [federico.alberini@unibo.it](mailto:federico.alberini@unibo.it) (F. Alberini).

<sup>1</sup> Permanent address: School of Construction Machinery, Chang'an University, 710064, Xi'an, China.

<https://doi.org/10.1016/j.cherd.2023.05.013>

0263-8762/© 2023 The Authors. Published by Elsevier Ltd on behalf of Institution of Chemical Engineers.

### Nomenclature

AR	aspect ratio $l/D$ [-]
$C_i$	local dimensionless conductivity [-]
$\bar{C}$	mean (in space) dimensionless conductivity [-]
$C_{t=0}^-$	mean (in time) local dimensionless conductivity before injection
$C_{t=\infty}^-$	mean (in time) local dimensionless conductivity after reaching steady state
CoV	coefficient of variation [-]
$D$	diameter of the mixing element and pipe [m]
$D_h$	hydraulic diameter [m]
$f$	friction factor [-]
$f_h$	friction factor, Eq. (3) [-]
$l$	length of the mixing element [m]
$L$	length of the mixing unit [m]
$L_e$	equivalent length [m]
$N$	number of the mixing element [-]
$Ne$	Newton number [-]
$Re$	Reynolds number [-]
$V$	effective fluid velocity [m/s]
$V_o$	superficial velocity [m/s]
$w$	mixing element thickness [m]
Greek letters	
$x$	normalized dimensionless conductivity [-]
$\varepsilon$	void fraction of the mixer [-]
$\mu$	fluid dynamic viscosity [Pa s]
$\rho$	fluid density [ $\text{kg m}^{-3}$ ]
$\Delta P_F$	distributed pressure drop [Pa]
$\Delta P_C$	concentrated pressure drop [Pa]

radial and tangential directions to the main flow (Ghanem et al., 2014) in laminar flow and they act as promoters of turbulence in turbulent flow. Static mixer is an attractive alternative compared with traditional agitation system, due to some obvious advantages, such as small space requirement, low equipment cost, self-cleaning (Thakur et al., 2003). More and more researchers are interested in the development of static mixers, which is proved by the increase of publication numbers related to this subject in the past ten years (Hosni et al., 2022).

Kenics static mixer (KSM) is a classical type of static mixer explored by many researchers also in recent works (Barkan-Öztürk et al., 2022; Nyande et al., 2022; Poumaëre et al., 2022). Pressure drop, flow characteristics and mixing performance are the focus of these research works.

In terms of experimental flow field characterization and mixing performance, Alberini et al. (2014) assessed the blending of Newtonian and time-independent non-Newtonian fluids in different working conditions using planar laser induced fluorescence (PLIF) and by imaging processing method. Ramsay et al. (2016) researched the mixing performance of ideal viscoelastic (Boger) fluids within KSM by PLIF technique, and coefficient of variance index and imaging processing method were used to assess homogeneity. In the turbulent regime, the effect of residence time and energy dissipation on drop size distribution for the dispersion of oil in water have been investigated using PLIF (Forte et al., 2019a). However, there are gaps on the experimental side, for the evaluation of mixing performance in particular in the turbulent regime.

Flow field and mixing performance have been also investigated by computational methods. Mahammed et al. (2017) explored pressure drop and velocity distribution in different working conditions under laminar flow using Computational Fluid Dynamics simulations. The effect of Reynolds number, fluid properties, twist angle and blade pitch on the flow characteristics and energy cost were evaluated. Murasiewicz and Zakrzewska (2019) investigated velocity distribution and heat transfer characteristics in KSM under turbulent flow by large eddy simulation. Based on discrete element method, Göbel et al. (2019) studied the impact of element number and angle of twist on the mixing performance of KSM, and twist angle of  $150^\circ$  and  $180^\circ$  had best performance in terms of mixing quality and mixing time. Haddadi et al. (2020) focused on droplet size distribution in turbulent dispersion of immiscible liquids using the Eulerian–Eulerian and Eulerian–Lagrangian approaches, and the residence time distribution of droplets was predicted.








In this work, the knowledge gap in the field of in-line monitoring for tubular reactors is covered from an experimental perspective focusing on the turbulent regime. The capabilities of a smart methodology and sensor technology towards energy-efficient mixing operations are explored. This is critical for process intensification of tubular reactors (Jegatheeswaran et al., 2018). The first part of the work concerns the development and the evaluation of a predictive model for pressure drop. Original and literature experimental data and previous correlations are used to check the reliability of the new mechanistic model. In the second part of the work, the results obtained from the pressure drop are interpreted observing the 2-D flow field of the pipe cross section at the outlet of the last element used for selected experiments. In the second part of the work, the results obtained from the pressure drop are interpreted observing the 2-D flow field measured at the outlet of the last element by Particle Image Velocimetry (PIV).

In the past few years, static mixers have been investigated by PIV in single phase (Alekseev et al., 2017), liquid-liquid (Voulgaropoulos and Angeli, 2017) and gas-liquid flows (Scala et al., 2020), but generally the application of PIV to the investigation of static mixing is less extensive with respect to the case of stirred tanks. To the best of our knowledge experimental data of the velocity field with Kenics static mixers are quite scant, with few contributions being the investigation of Van Wageningen et al., (2004) and Murasiewicz, Jaworski (2013), which reported Laser Doppler Anemometry measurements.

Finally, the mixing performances are evaluated by the application of Electrical Resistance Tomography (ERT), which has been widely adopted for the investigation of fluid mixing in stirred tanks, particularly in multiphase flow (e.g. Maluta et al., 2020) and in a few cases also in reacting systems (Alberini et al., 2021), while the application to tubular reactors are scant (Forte et al., 2019b; Jegatheeswaran et al., 2018). Overall, pressure drop, velocity field and tracer homogenization data are analysed to provide deep insight into the effects of varying mixing conditions and static mixing elements arrangement in a tubular reactor with the final purpose to guide towards the enhancement of continuous operations based on the pressure drop control and the online monitoring by a smart sensor such ERT.



**Table 1 – Static mixer configurations<sup>\*\*</sup> investigated in this work.**

Configurations	C	C-C	A	A-C	C-A-C
					
					
					

<sup>\*\*</sup> Since the flow direction is from right to left, the mixer configuration is named with the first element corresponding to the downstream one. A elements are depicted in grey while C elements are depicted in white.

were performed with all the single and the double elements configurations, the velocity field was measured with configurations A, A-A, and C-A, the liquid mixing was measured with configurations A, C, A-A, C-A and C-A-C.

Demineralized water at the room temperature of  $20\text{ }^{\circ}\text{C} \pm 2\text{ }^{\circ}\text{C}$  was used in most of the experiments. The investigated flow rates and the corresponding operating Reynolds number,  $Re$ , adopted for the pressure drop measurements are listed in Table 2. The ERT and PIV data were collected at  $Re=9972$  only.

To extend the pressure drop analysis additional tests, at ambient temperature, with a water-glycerol solution were performed. The density of the mixture was  $1210\text{ kg/m}^3$  while the dynamic viscosity was equal to  $0.106\text{ Pa}\cdot\text{s}$ . The liquid flowrates were equal to those used for water experiments, but the operating Reynolds number moved to the range 12–144.

### 2.1. Particle image velocimetry

The mean velocity field was measured on a plane perpendicular to the axial direction of the pipe and located 11 mm downstream the static element(s) outlet, that was always placed at 782.5 mm from the pipe inlet. As shown in Fig. 1(a), the laser light sheet entered the pipe through a flat window, to avoid deviations due to the pipe curvature. The camera was set perpendicularly to the laser light sheet, to this end the pipe was provided with an acrylic window opposite to the inlet section.

The PIV instrumentation consisted of a pulsed Nd: YAG laser (Solo I-15 Hz, 15 mJ New wave research, US), emitting light at 532 nm with a maximum frequency of 15 Hz, a HiSense MkII CCD camera ( $1344 \times 1024$  pixel resolution) provided with a optical green filter to capture only the light emitted by the laser source and scattered by the seeding particles, a hardware module (FlowMap System Hub, Dantec Dynamics) for the laser control, the laser/camera synchronization and the data acquisition, the FlowManager software (Dantec Dynamics) for data processing. Talc particles (diameter:  $1.7\text{ }\mu\text{m}$ , density:  $2820\text{ kg/m}^3$ ) with a relaxation time

equal to  $4.5 \times 10^{-7}$  s, were used for seeding the liquid (Paglianti and Montante, 2020).

The time interval between two laser pulses,  $\Delta t$ , of  $40\text{ }\mu\text{s}$  was adopted for minimizing the error due to the out-of-plane movement of the seeding particles, based on the analysis of preliminary data. For each measurement, a total number of image pairs of 800 was acquired; this number was selected since it ensured the statistical independency of the mean velocity data. The acquisition frequency was equal to 1 Hz.

The velocity vectors were obtained by applying the cross-correlation to the image pairs with an interrogation area size of  $32 \times 32$  pixels ( $0.96 \times 0.96\text{ mm}$ ) with overlap of 50%. The cross-correlation was applied to each image pair after removing the environmental light noise obtained from the average of the instantaneous images (Yao et al., 2023). This is useful to reduce the noise in the raw PIV image. The mean velocities were calculated from the instantaneous vectors after the following steps of postprocessing were performed. The vectors were discarded if they did not fulfil two conditions: one based on the evaluation of the peak heights in the correlation plane and the other on the velocity magnitude (Paglianti and Montante, 2020). The perspective error due to the out of plane component can be estimated using the approach suggested by Yoon and Lee (2002) and depends from the relative value between the out of plane and the in plane component and the angle subtended by the particle position and the axis of the recording device, that in present experiments is maintained as small as possible and equal to  $1.35^{\circ}$ .

### 2.2. Electrical resistance tomography

ERT technique was used to evaluate the mixing performances (Wang et al., 1996) based on the variation of the liquid conductivity along the length of the tubular reactor. The experiments were carried out feeding two iso-kinetic liquid streams with different conductivity, resulting in the same total flow rate adopted for the PIV measurements. The main liquid stream was fed as described in Section 2, the secondary feed, that is added by using a hydrostatic column head of 4 m, in order to maintain isokinetic conditions ( $5\text{ L/h}$ ); it was delivered in the centre of the inlet section by a tube of diameter equal to 2 mm. The secondary stream flow rate was fixed with a glass tube rotameter, measuring in the range  $0\text{--}50\text{ L/h}$ . In the two streams, a different concentration of NaCl was preliminary dissolved, namely  $2\text{ g/L}$  and  $80\text{ g/L}$  in the mean and the secondary stream respectively, thus enabling the detection of the homogenization dynamics by the

**Table 2 – Flow rates and  $Re$  used for the pressure drop measurement using water as working fluid.**

Flow rate [L/h]	469	620	968	1468	1967
$Re$	7518	9972	15526	23533	31541



ERT system. In both cases, the salt was assumed to negligibly affect the viscosity and the density of the liquid.

The conductivity data were collected by the ERT instrument P2000 and recorded and analysed with the software p2 + V9 and with the software Sensitivity Conjugate Gradient (SGC) version 2.59 (Wang, 2002), both provided from Industrial Tomography Systems Ltd., UK,. The measurements were performed adopting the circular adjacent strategy, by the injection of electric current of amplitude equal to 15 mA and frequency of 9600 Hz from an adjacent electrode pair at a time and on the measurement of the voltage difference from the remaining pairs of electrodes. The local conductivity, 316 values per plane, was obtained from the voltage measurements in real time both by the linearized (non-iterative) modified sensitivity back projection (MSBP) algorithm, when the P2 + V9 software was used, and by the iterative Sensitivity conjugate gradients algorithm, when the SGC software was used.

The measured variable is the dimensionless conductivity in the cell  $i$ ,  $C_i$ , calculated as the conductivity during the secondary stream feeding divided by the reference conductivity. The reference conductivity was measured before the feeding of the secondary stream.

The values of amplitude and frequency of the injected current were selected to optimize the signal-to-noise ratio (SNR) of the measured voltage outputs, which depends on several variables, including the liquid conductivity, the pipe size, and the pipe material.

The data rate was 1.66 frames per second, corresponding to a temporal resolution of 0.60 s. The sources of ERT measurement uncertainties are electronic noise and liquid temperature variations.

### 2.2.1. Implementation and calibration tests of the ERT's pipe double plane sensors

A novel type of electrodes consisting of 304 stainless steel bolts with a diameter of 3 mm suitable to the small pipe size has been devised, following the structure of sensor planes commonly used for cylindrical geometry, as shown in Fig. 1(a). The electrodes set up is similar to that previously adopted by Hou et al. (2016). The main difference is due to the length and the shape of the measuring sections. They are 1D length and can be mounted between any of the flanges of the experimental rig. The small length of the measuring sections allows to perform the mechanical work necessary to assure the thread flush with the inside surface of the pipe. Moreover, this set-up allows to easily move the measuring section along the pipelines. The ERT's pipe double plane sensor (ERT-pipe) consisted of two rows of 16 bolts equally spaced in the perimeter of the external circumference of the pipe. The pipe was provided with 34 holes required for fixing the 32 electrodes and one extra electrode for the earths of each plane, located at one pipe diameter from the relative sensor plane. The bolts were glued to the external wall of the pipe to avoid any glue covering the surface of the electrode in contact with the fluid and to ensure water tightness of the sensor planes. The two planes, in the following  $z_1$  and  $z_2$ , were one at 80 mm from the other with the downstream one placed at 7 mm from the last element outlet, as shown in Fig. 1(a).

Before carrying on the experiments, tests adopting three phantoms, two consisting of metal rods of diameter  $d_{r1}=4$  mm and  $d_{r2}=6$  mm and one in plastic of diameter  $d_{r3}=6$  mm were performed in the pipe filled with the salty water in still condition, to make sure that the bolts were

suitable to provide trustful results. The metal/plastic rod was inserted in the centre of the tube, ensuring that the rod axis was parallel to the tube axis. Furthermore, some tests with one sensor plane filled with salted water and non-conductive Polyoxymethylene particles were performed. The particles, with diameter equal to 5 mm were added up to the maximum possible number. The goal of the latter test was to mimic a condition in which the non-conductive material was distributed on the whole volume and not concentrated in a single point.

The dimensionless conductivity maps obtained with the different tests are shown in Fig. 2. On the left the results obtained with MSBP algorithm while on the right the results obtained with SGC algorithm are shown. The number of the iterations to achieve the non-linear solution with a mesh of 1600 elements was in each case equal to 15.

The dimensionless conductivity was obtained as the ratio between the conductivity in the pipe measured with and without the rod. The increase of red area corresponding to the higher values of dimensionless conductivity indicates that the sensor correctly detects the two different sizes of the metal rods.

The experimental data, depicted in Fig. 2, clearly show how the boundary of a single phantom set in the measuring section is identified. Clearly, the sensitivity conjugate gradient approach is necessary for the presence of strong gradients, while if the non-conductivity material is distributed in the whole cross section (Fig. 2d) the differences between the results obtained with the two approaches are less evident. Table 3 reports the Coefficient of variation of the dimensionless conductivity computed for the four analyzed cases.

Thus, the Coefficient of variation significantly differs between the two methodology only when a single concentrated phantom is present. Then, it is possible to conclude that SGC algorithm is recommended for the evaluation of the local conductivity in the sections close to the inlet of the secondary stream. Here, the two streams are not fully mixed yet. While in the downstream sections, within and after the mixing elements, the MSBP can be used.

In present work ERT has been used to quantify the mixing performances obtainable when two streams with different salt content are mixed in a pipeline equipped with static mixers. The following plot (Fig. 3) reports the calibration showing that the measured average conductivity in the measuring plane linearly depends from the salt concentration.

### 2.3. The mechanistic model for the pressure drop prediction

Correlations for the pressure drop estimation in pipelines equipped with KSM working in single phase flow are already available in the literature. The pressure drop is often evaluated in terms of Newton number,  $Ne$ , as a function of the operating Reynolds number,  $Re$  (Jiang et al., 2021; Thakur et al., 2003b; Pahl and Muschelknautz, 1982; Streiff, 1979; Etchells and Meyer, 2004; Streiff et al., 1999). The Newton number is a dimensionless ratio between the resistance due to the friction and the inertia forces. The  $Ne$  and the  $Re$  are usually defined as:

$$Ne = \frac{\Delta P D}{\rho V_o^2 L} \quad (1)$$

$$Re = \frac{D \rho V_o}{\mu} \quad (2)$$

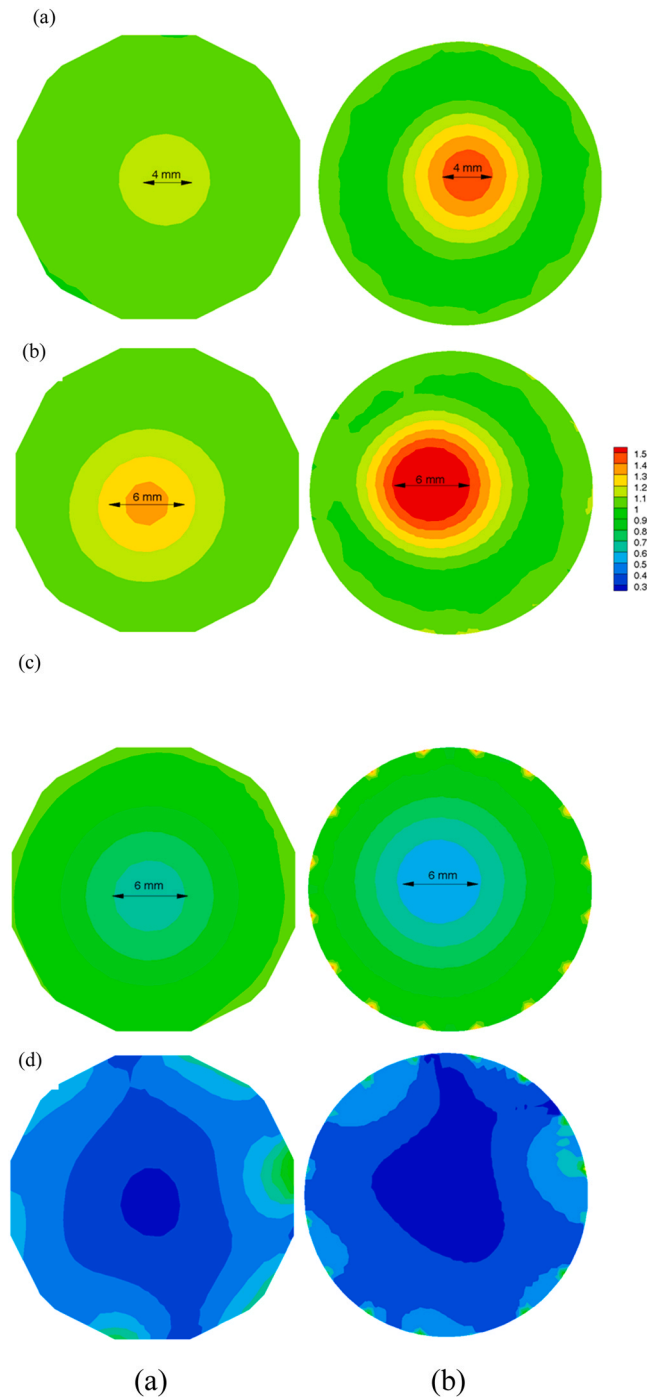


**Fig. 2 – Dimensionless conductivity reconstruction with the metal rods (a)  $d_{r1}= 4$  mm metal and (b)  $d_{r2}= 6$  mm metal (c)  $d_{r3}= 6$  mm plastic, (d) plastic spheres. On the left the reconstruction obtained with MSBP algorithm and on the right the reconstruction obtained with the SGC algorithm.**

Table 3 – Coefficient of variation obtained with the phantom tests.		
Type of phantom	MSBP algorithm	SGC algorithm
4 mm metal	0.04	0.12
6 mm metal	0.07	0.16
6 mm plastic	0.11	0.17
Spheres	0.24	0.26

Where  $D$  is the pipeline diameter,  $L$  is the total length of the mixing unit,  $V_0$  is the liquid superficial velocity,  $\rho$  is the fluid density,  $\mu$  is the fluid viscosity and  $\Delta P$  is the pressure drop.

In other cases, instead of the friction factor,  $f$ , that is equal to  $Ne/2$ , the friction factor based on the equivalent diameter of the channel,  $f_h$ , (Theron and Sauze, 2011) is considered:

$$f_h = \frac{\Delta P \epsilon^2 D_h}{2 \rho V_0^2 L} \tag{3}$$

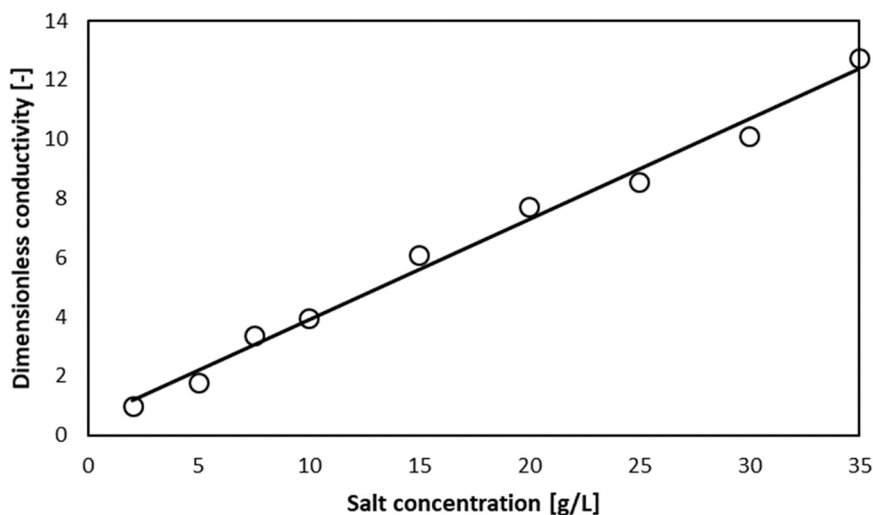


Fig. 3 – Effect of the salt concentration on the dimensionless conductivity. Static calibration reference measured with 2 g/L of NaCl.

Where  $\varepsilon$  is the void fraction of the mixer,  $D_h = 4S/P$  is the hydraulic diameter of the channels of the mixer (Streiff et al., 1999),  $S$  is the surface available for the liquid flow and  $P$  is the wetted perimeter. As a result, the hydraulic diameter is calculated as:

$$D_h = \frac{4\left(\frac{\pi D^2}{4} - Dw\right)}{(\pi D - 2w + 2D)} = \frac{\pi D - 4w}{\pi + 2 - 2\frac{w}{D}} \quad (4)$$

Where  $w/D$  is the ratio between the mixing element thickness,  $w$ , and the pipe diameter,  $D$ .

In this work an alternative model based on distributed and concentrated pressure drop is proposed, similarly to what proposed for estimating the pressure drop in pipelines equipped with SMV static mixers (Paglianti and Montante, 2013). This model offers the possibility of easily predicting the pressure drop in case of scale-up of a tubular reactor equipped with static mixers and also of considering the effect of alternating type of static mixer geometry (for example a combination of C and A). From the energetic efficiency perspective, a reliable and versatile correlation for the estimation of pressure drop in a wide range of conditions is crucial for process optimization.

The prediction model assumes that the overall frictional pressure drop,  $\Delta P$ , is determined by the following main contributions:

(a) The distributed pressure drop,  $\Delta P_F$ , due to the friction between the fluid and the mixer walls;

(b) The concentrated pressure drop,  $\Delta P_C$ , at the inlet, at the outlet and at the surface between two consecutive elements.

For steady state condition of an incompressible single phase flowing in horizontal pipe, both the acceleration and gravity effects can be neglected. In applications where these contributions are essential, they can be included in the model, as in the columns equipped with structured packings (Brunazzi and Paglianti, 1997).

Based on these hypotheses, the overall pressure drop can be written as:

$$\Delta P = \Delta P_F + \sum_{i=1}^{N+1} \Delta P_{C,i} \quad (5)$$

Where  $\Delta P_F$  indicates the value of the distributed pressure drop. It is worthwhile noticing that the number of the concentrated pressure drop terms,  $\Delta P_{C,i}$ , is equal to the number of mixing elements,  $N$ , plus 1. In fact, it is necessary to estimate the concentrated pressure drop between two consecutive elements, equal to  $N-1$  terms, and the inlet and outlet effects, equal to two terms.

In order to calculate these contributions, empirical parameters, i.e. the friction factor and the equivalent length associated to the concentrated pressure drop, that depend on the geometrical characteristic of the single mixing element, must be defined.

### 2.3.1. The distributed pressure drop

The distributed frictional loss term,  $\Delta P_F$ , can be evaluated by the energy balance on the fluid flowing in a single channel composing the static mixer as:

$$\Delta P_F = 4f \frac{L}{D_h} \rho \frac{V^2}{2} \quad (6)$$

where  $D_h$ , is the hydraulic diameter,  $f$  is the friction factor and  $V$  is the effective fluid velocity, defined as:

$$V = \frac{V_0}{\varepsilon} \quad (7)$$

It is worth observing that the effective velocity depends on the void fraction of static mixer,  $\varepsilon$ , which can be computed as:

$$\varepsilon = \frac{\frac{\pi D^2}{4} - wD}{\frac{\pi D^2}{4}} = \frac{D - \frac{4w}{\pi}}{D} \quad (8)$$

Where  $w$  is the static mixer thickness.

For the friction factor  $f$ , a semi-empirical relation has been adopted:

$$\begin{aligned} f &= 16/Re \text{ for laminar flow, } Re < 100 \\ f &= 1.6 Re^{-0.5} \text{ for transitional flow, } 100 < Re < 1000 \\ f &= 0.05 \text{ for turbulent flow, } Re > 1000 \end{aligned} \quad (9)$$

The above equations have been fixed analysing both present and previous experimental data (Yao et al. 2023, Hosni et al. 2022, Kumar et al. 2008).

### 2.3.2. The concentrated pressure drop

The concentrated pressure drop taken into account is located at the inlet section, at the outlet section and in the section between one element and the following. The overall contribution is estimated as:

$$\Delta P_C = \sum_{i=1}^{N+1} 4f \frac{Le_i}{D_h} \rho \frac{V^2}{2} \quad (10)$$

Where  $Le_i$  is the equivalent channel length corresponding to each  $i$  concentrated pressure drop and  $N$  is the number of the mixing elements.

The inlet and the outlet pressure drop can be evaluated as:

$$\Delta P_{C,inlet} + \Delta P_{C,outlet} = 4f \frac{Le_{inlet} + Le_{outlet}}{D_h} \rho \frac{V^2}{2} \quad (11)$$

Where the friction factor,  $f$ , can be computed by Eq. (9).

The equivalent length depends on the inclination of the internal blade, and on the ratio of the element length and the pipe diameter. In this work we analysed only elements with length equal to 1.5 times the pipe diameter, but the model can be adapted to analyse different geometries also, e.g static mixers with different aspect ratio (AR) or different twist angle.

The pressure drop at the interface between two consecutive elements depends on their relative position. Here two different arrangements have been considered: (a) mixing elements inserted alternating A and C types; (b) mixing elements of one type only.

The parameters used for evaluating the pressure drop obtained in present work are listed in Table 4.

## 3. Results and discussion

### 3.1. The pressure drop

In Fig. 4(a) the pressure drop measured using water as working fluids are plotted versus the Reynolds number. As expected, the pressure drop increases at increasing  $Re$  with a different trend depending on the mixing element arrangement. The pressure drop increases with the number of elements, but it is not affected from the element type, as can be observed from the coincident results measured with a single C or A element or two consecutive identical elements (C-C and A-A configurations). Differently, when the type of elements is mixed, there is a significant increase of pressure drop compared to the configuration with the same type, while maintaining similarity for the same sequence (configuration CA or AC). In Fig. 4(b), the measured pressure drop values are compared with the results of the model presented in Section 3 in a parity plot. Overall, the model seems to predict reasonably well all the conditions with lower performance for the single element.

**Table 4 – Parameters for concentrated pressure drop.**

Concentrated pressure drop	$Le/D_h$
Inlet+outlet	1.88
Alternating C and A elements	8.29
Same element type	0.10

To widen the model evaluation, the comparison has been extended to literature data. The first comparison shown in Fig. 4(c) concerns a tubular reactor (Yao et al., 2023) of pipe diameter equal to 39.5 mm, AR=1.5, and similar geometry of the static elements. The second comparison, shown in Fig. 4(d), reports the data collected by Hosni et al. (2021) in a pipe of 40 mm, AR=1.5, in diameter and up to 6 static elements. The comparison with the data of Kumar et al. (2008) is shown in Fig. 4(e) the data are collected in a 25.4 mm tube, AR=1.5, provided with up to 25 static elements. In Fig. 4(e) the comparison has been extended to a fluid with different physical properties respect to water. For all the comparisons the performance of the model is acceptable. Therefore, the proposed model can be an useful tool for evaluating the pressure drop, even if other tests with different fluids are recommended.

### 3.2. The velocity field

To better understand the implications of using different configurations of the static mixer and the difference in the pressure drop, the flow field measured in the cross section just downstream of the last element is analysed in the following. The cross section is considered since the mixing characteristics are mainly affected by the radial and tangential flow components. The mean error induced by the presence of the out of plane component can be estimated as 5% of the in plane component. The experimental data are presented in Fig. 5. For a single anti-clockwise element (A), from the results shown in Fig. 5(a-b), it is clear that the centre of the pipe is characterized by a zone with a low velocity magnitude. The higher velocities are located in two zones, one on top of the other, and the pattern of the vectors is consistent with the anti-clockwise direction of the element. With the increase of the number of elements, the zones of higher velocity are smaller, as can be observed from the results shown in Fig. 5(c-d) and (e-f). Comparing the velocity magnitude obtained with the single elements with that of two elements shown in Fig. 5(c) and (e) and with the histograms of Fig. 5(d) and (f), it is apparent that the number of vectors in the higher velocity magnitude range decreases moving from the configuration A to A-A and it decreases even further with the configuration C-A. Overall, the more homogeneous velocity distribution is obtained in the tubular reactor equipped with multiple mixing element respect to the case with a single element. As expected, the different rotation of the consecutive elements induces a flow field variation. Obviously, different orientation of the mixing elements influences also the pressure drop.

### 3.3. Transient and steady state fluid mixing characteristics

The final step of this work is to investigate the mixing performances of the tubular reactor based on the non-intrusive monitoring of the mixing evolution in time and along the reactor length. The method can be easily implemented in a real industrial process, providing a step ahead towards smarter control and optimization of continuous reactors.

The analysis of the transient regime is performed first, considering the time interval between the onset of the secondary stream feeding and the achievement of the steady



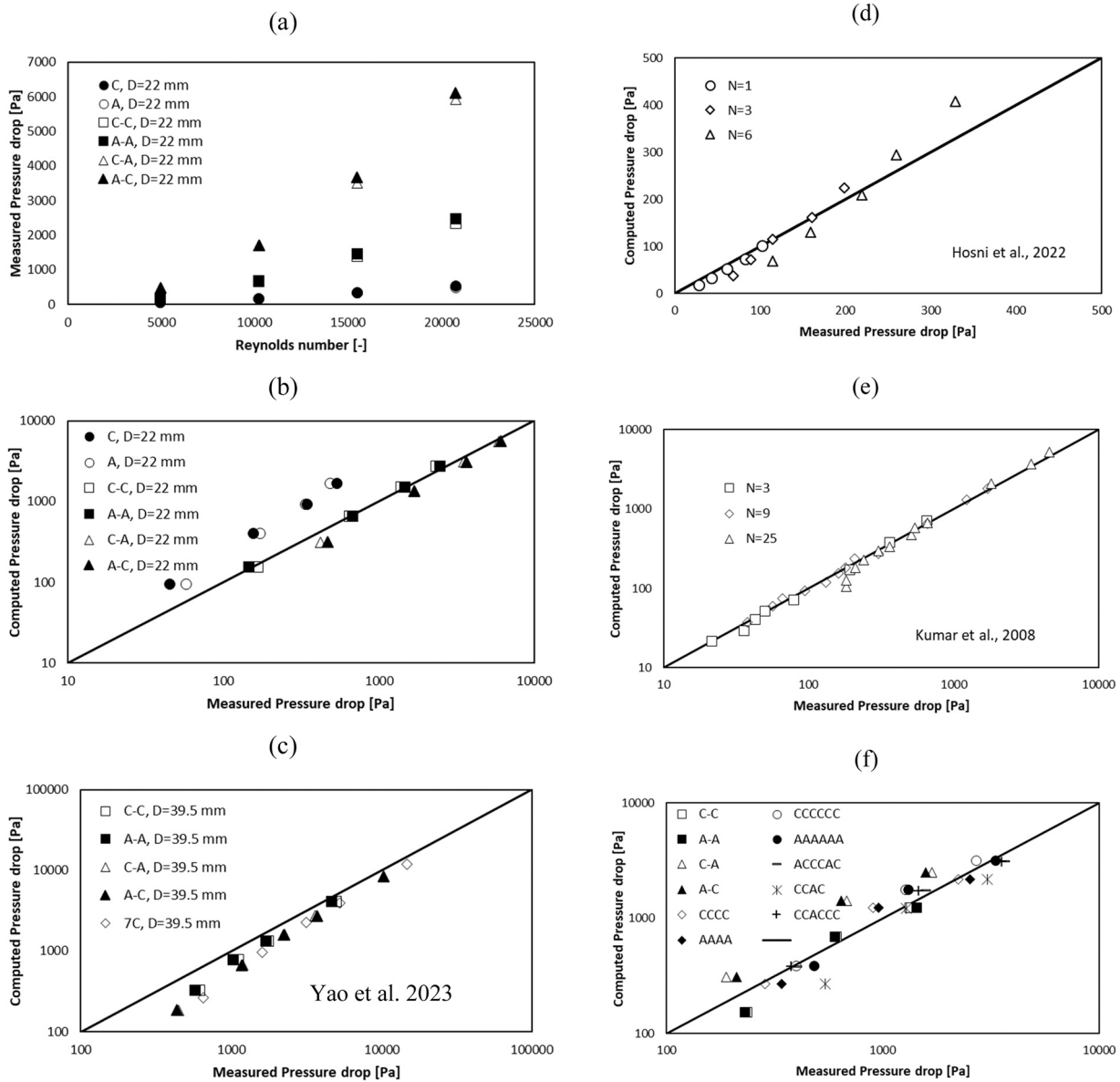


**Fig. 4 – Comparison of computed and experimental data: (a) effect of the Reynolds number and of the mixing element set-up on the measured pressure drop. D= 22 mm, AR= 1.5 water (b)D= 22 mm, AR= 1.5 current work, water (c) D= 39.5 mm, AR= 1.5 data by Yao et al. (2023) (d) D= 40 mm, AR= 1.5 data by Hosni et al. (2022) (e) D= 25.4 mm, AR= 1.5 data by Kumar et al. (2008) (f) D= 22 mm, AR= 1.5 current work, water-glycerol solution.**

state condition. The local normalized dimensionless conductivity is calculated as:

$$x_{i,t} = \frac{C_i - C_{t=0}^-}{C_{t=\infty}^- - C_{t=0}^-} \tag{12}$$

Where  $C_{t=0}^-$  and  $C_{t=\infty}^-$  are the local dimensionless conductivity, before feeding the secondary stream and after the achievement of the steady state condition, respectively.

In Fig. 6 and Fig. 7, the time evolution of the local normalized dimensionless conductivity has been plotted for the cases of a single static mixing element (A) and for the combination of two elements (C-A). The comparison between the two conditions allows to quantify the positive effect on the mixing performances obtained with the C-A with respect to the A configuration.

Fig. 8 shows the evolution of the average local con-

ductivity in the case of a single clockwise element (C) after the feeding of secondary stream. As can be observed, the conductivity achieves a steady state value after about 40 s from the secondary feeding onset. It is worthwhile noticing that the characteristic time for achieving the steady state is much greater than the filling time of the pipe, computed as the ratio between the pipe volume and the volumetric flow-rate fed to the loop.

In order to identify the number of frames ensuring a sample independent average conductivity, the values obtained from the average of a different number of instantaneous frames collected 60 s after starting the feeding of the secondary stream are compared in Fig. 9, where the average values in the diametrical line of the measurement section are shown. As can be observed, increasing the number of frames the average values tend to converge to

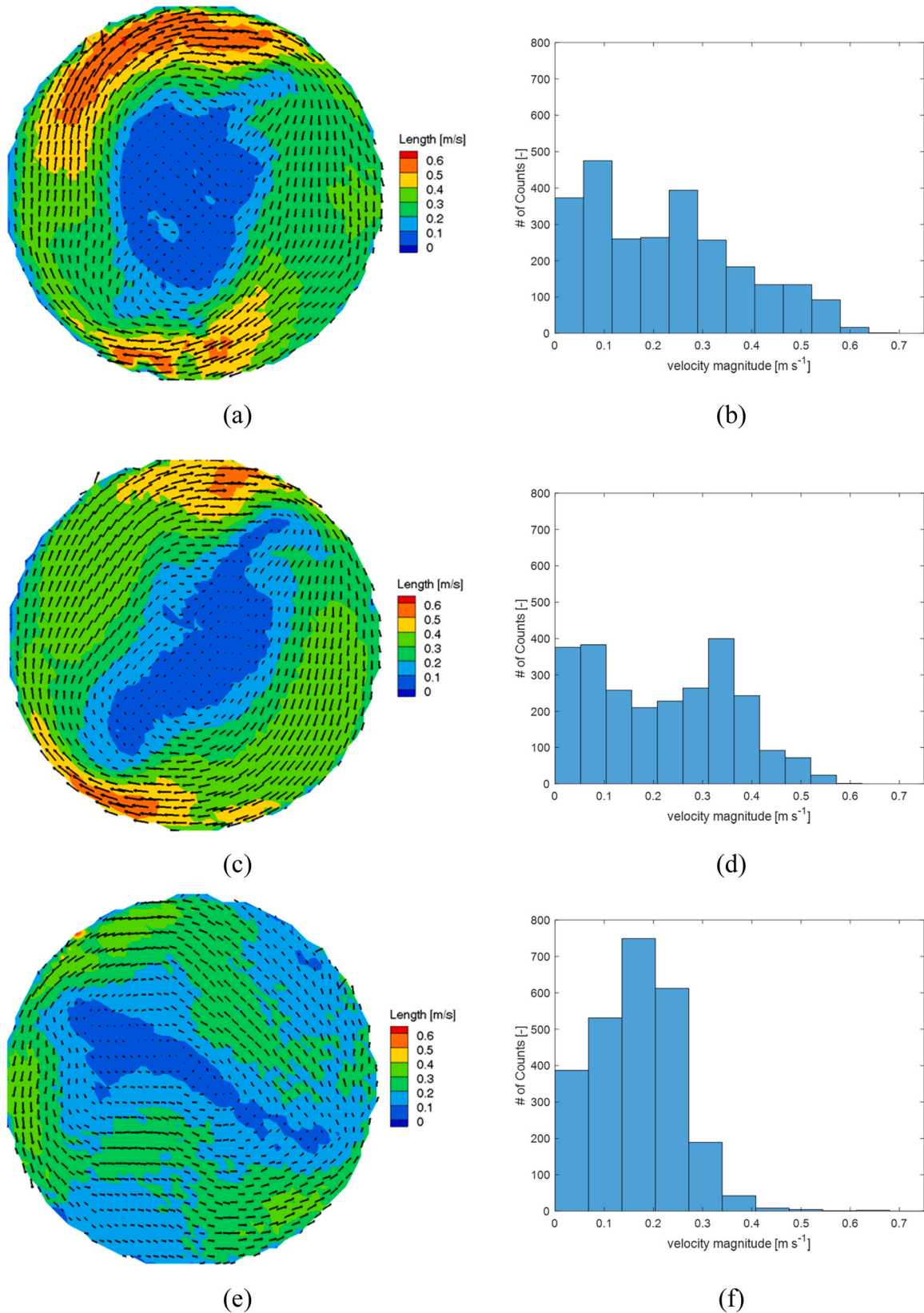


**Fig. 5 – PIV data: Map of velocity magnitude and velocity vector plot (a) A; (c) A-A; (e) C-A and velocity magnitude distributions (b) A; (d) A-A; (f) C-A. Reynolds number equal to 9972, the color scale is in [m/s].**

single values for each location and at least 150 frames are necessary to obtain a constant average conductivity from the instantaneous samples.

Based on the results shown in Figs. 8 and 9, the comparison of the investigated configurations, which is focused on the steady state working conditions, refer to the average of 150 instantaneous normalized dimensionless conductivity

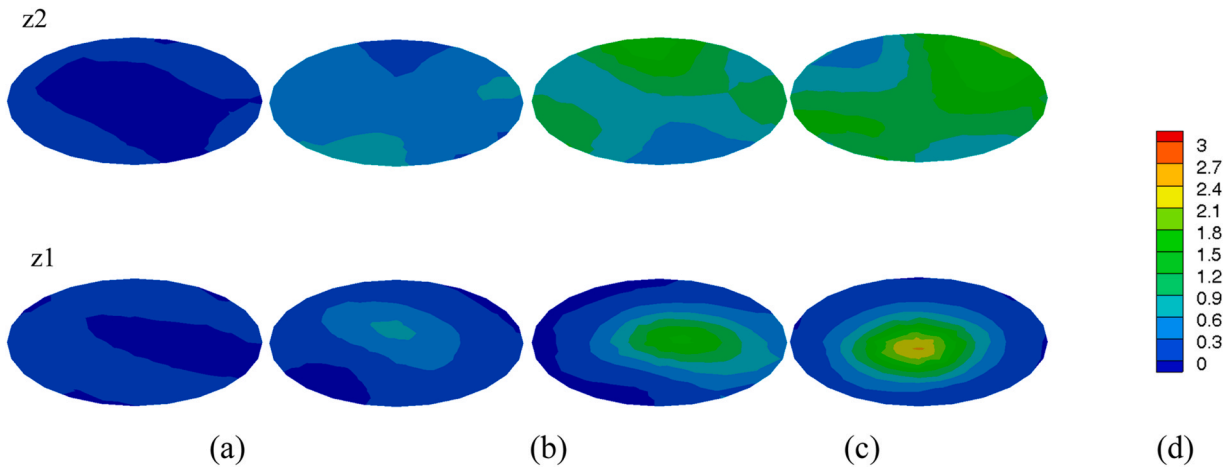


Fig. 6 – Normalized dimensionless conductivity maps obtained with A: (a)  $t = 0$ ; (b)  $t = 2.00$  s; (c)  $t = 4.00$  s; (d)  $t = 6.00$  s. Reynolds number equal to 9972.

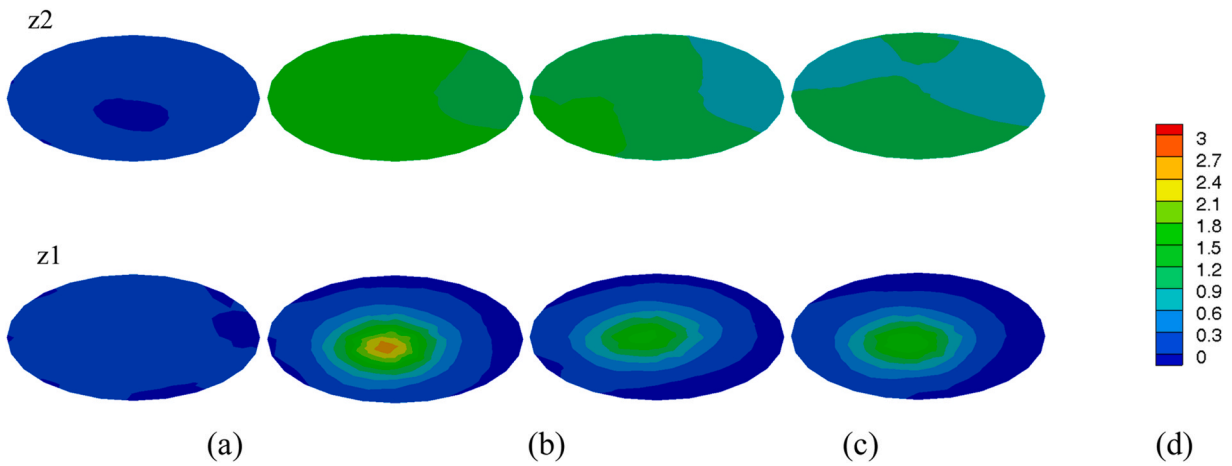


Fig. 7 – Normalized dimensionless conductivity maps obtained with C-A: (a)  $t = 0$ ; (b)  $t = 2.00$  s; (c)  $t = 4.00$  s; (d)  $t = 6.00$  s. Reynolds number equal to 9972.

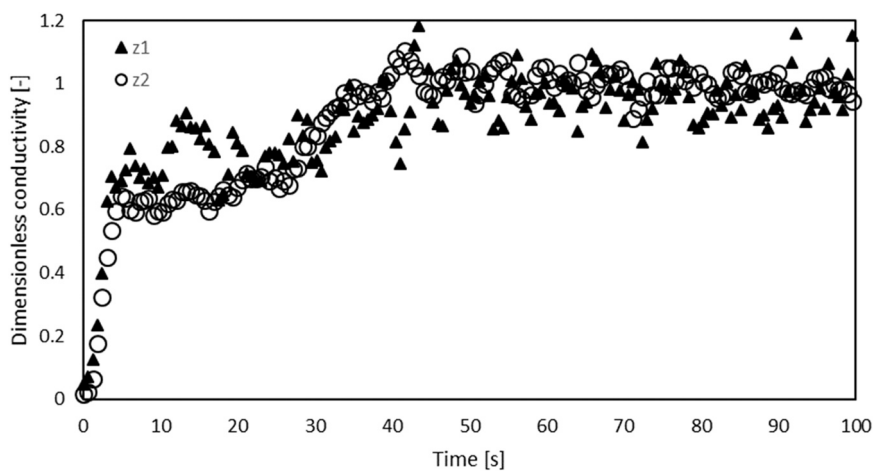
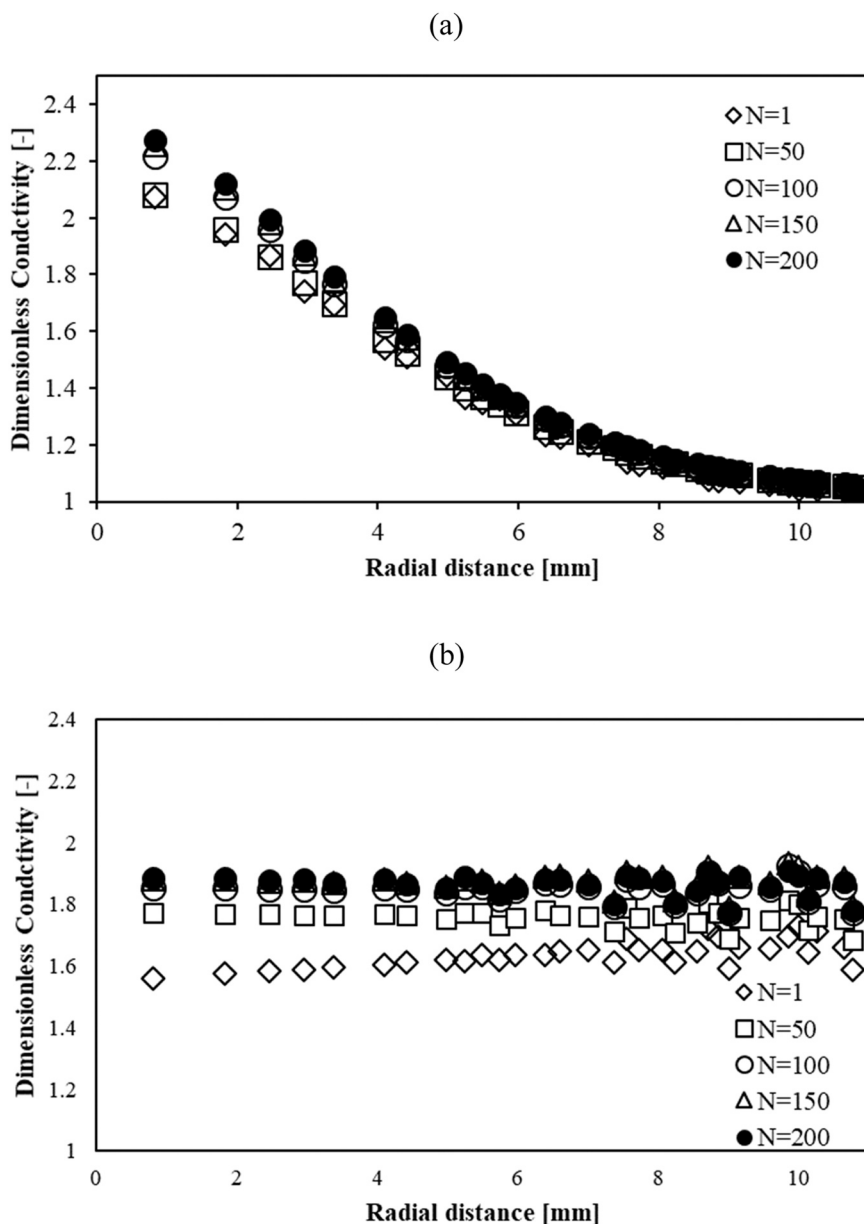


Fig. 8 – Time series of the plane average normalized dimensionless conductivity. Configuration (C). Reynolds number equal to 9972.

maps collected after 60 s from the secondary stream addition. The value of the mean normalized conductivity on the section if the mixture is perfectly mixed is 1.81.

The maps in Fig. 10 show the results on the two measurement planes. For the empty pipe, single and double element configurations shown in Fig. 10 (a)-(e), z1 was located



**Fig. 9 – Radial profiles of dimensionless conductivity obtained from the average of a different number of frames. Configuration (C), Plane z1 (a) z2 (b). Reynolds number equal to 9972.**

upstream of the first mixing element, while with the configuration including three elements shown in Fig. 10 (f), it was inside the first element. In all cases, z2 was located downstream of the latter mixing element. The maps are consistent with the expected increase of the homogenization quality with the increase of the element numbers, including the z1 plane map for configuration C-A-C, which confirm the reliability of the method to gain information in the optical inaccessible sections located inside the mixing elements.

Finally, the mixing performances are evaluated observing the Coefficient of Variation of the local dimensionless conductivity and also of the average velocity (shown in Fig. 5) calculated as:

$$CoV = \sqrt{\frac{\sum_{i=1}^N (C_i - \bar{C})^2}{\bar{C}^2 (N - 1)}} \quad (13)$$

Where  $\bar{C}$  is the mean value of the dimensionless conductivity in the cross section ( or  $\bar{V}$  the equivalent for the CoV of the velocity) on the measuring cross-section.

The overall results are summarized in Fig. 11, where the CoV evaluated in the mixers downstream section is depicted. All the measurements have been performed in triplicates and the minimum CoV value measured upstream the first mixer was 0.21, while the maximum value was 0.24 for the conductivity. For the CoV of velocity, the variation is related to the distribution of velocities in the cross section. More changes in the flow are induced by the different orientations of the static mixer, less variations, related to the mean cross sectional velocity, are depicted. The CoV data evaluated downstream of the mixers allow to quantify the quality of the homogenization process, which increases with the number of static mixers. It is worthwhile noticing that the



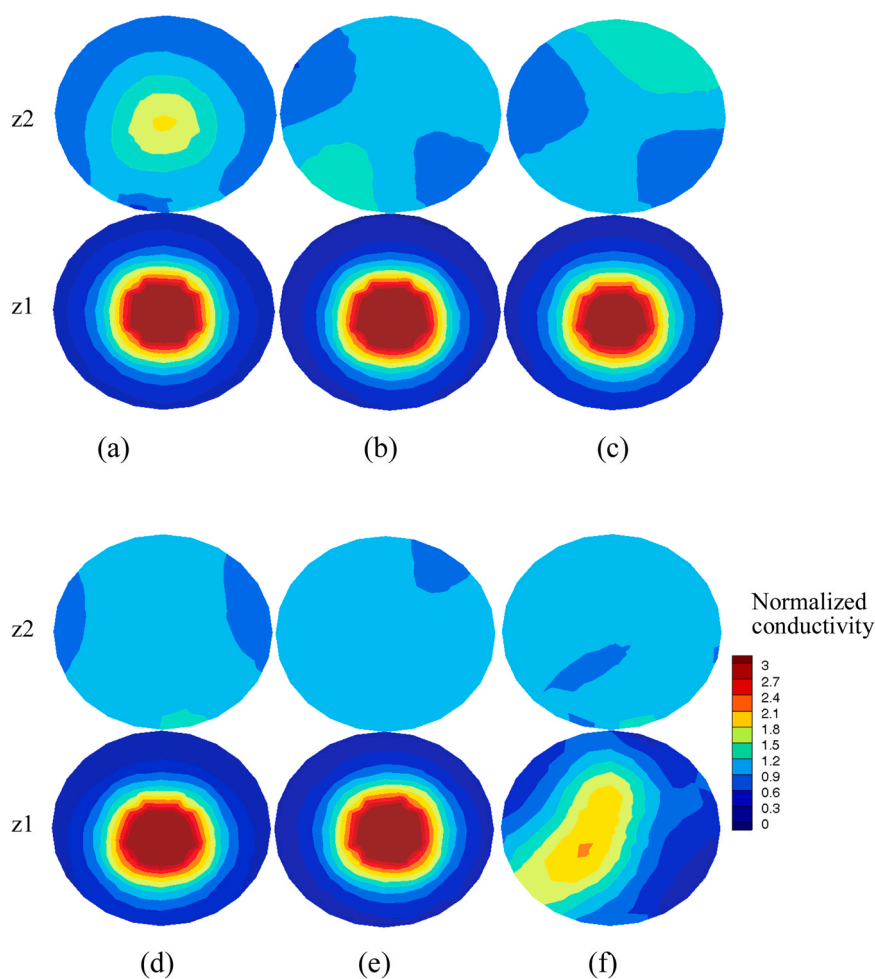


Fig. 10 – Normalized dimensionless conductivity maps obtained under steady state conditions in different configurations: (a) empty pipe; (b) C; (c) A; (d) A-A; (e) C-A; (f) C-A-C. Reynolds number equal to 9972.

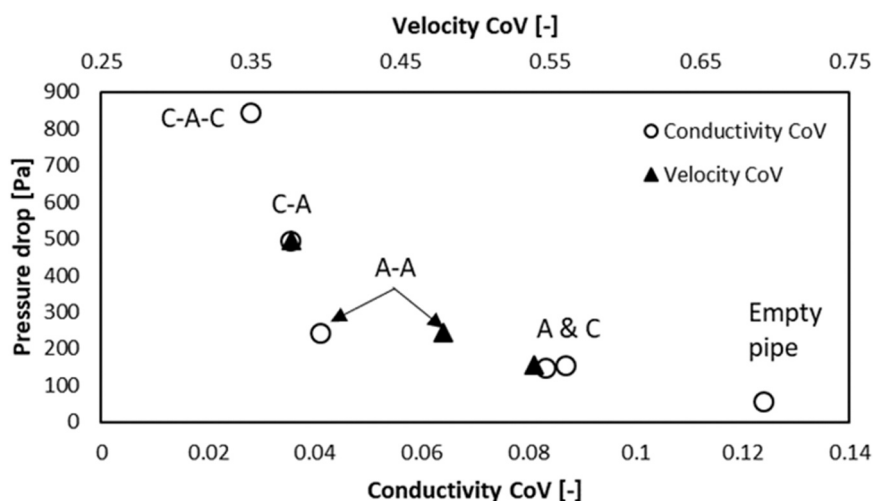


Fig. 11 – CoV vs pressure drop values: empty-pipe; A; C; A-A; C-A; C-A-C. Reynolds number equal to 9972,.

CoV value of the A-A configuration does not differ significantly from the C-A. Therefore, for limiting the pressure drop, in turbulent conditions, the use of mixing elements with the same orientation could be considered.

#### 4. Conclusions

In this work, an experimental analysis on the fluid dynamics behaviour of a tubular reactor equipped with KSM elements

has been performed. Two advanced techniques, Electrical Resistance Tomography and Particle Image Velocimetry, have been applied for the investigation. For the ERT application, a new set-up of the measuring probe allowing to analyse the behaviour of pipe with a small diameter is suggested. The impacts of element combinations on pressure drop, velocity distribution and mixing performance were experimentally evaluated. Furthermore, a new correlation for the prediction of pressure drop based on the distributed

pressure drop and concentrated pressure drop was proposed. The key conclusions are as follows:

1) The proposed correlation, which accounts for distributed and concentrated pressure drop, allows to estimate the effect of the relative position between consecutive mixing elements. The prediction of the pressure drop in pipeline with KSM with different set-ups, different working conditions and different working fluids provides acceptable results. The model is tested with current work and available in the literature data, showing the robustness of the model. The absolute performance of the model has room of improvement with the contribution of the research community generating more experimental data.

(2) ERT technique can successfully evaluate the mixing performance of KSM. ERT can assess the mixing performance in the middle of KSM, which is difficult to obtain by optical methods and it can provide important guideline for the selection of optimal trade-off between energy consumption and mixing efficiency.

(3) The effects of the relative position of two consecutive static mixer elements on the mixing performances has been quantified. This information, together with the prediction of the pressure drop, can be used for the optimization of the process. By using ERT, that can be implemented online and in a non-intrusive way, continuous reactors can be monitored to improve the energetic efficiency and the mixing performances of industrial operations.

## Ethical Approval

Not applicable.

## Funding

Z. C. Yao gratefully acknowledges the financial support for his stay at the University of Bologna from Fundamental Research Funds for the Central Universities, CHD, China (300102251711) and China Scholarship Council, China (202006560027).

## CRedit authorship contribution statement

**Yao Zechen**: Methodology, Experimental campaign, Writing – original draft. **Federico Alberini**: Supervision, Conceptualization, Investigation, Writing – review & editing. **Giuseppina Montante**: Conceptualization, Supervision, Writing – review & editing. **Alessandro Paglianti**: Conceptualization, Supervision, Writing – review & editing.

## Availability of data and materials

Not applicable.

## Declaration of Competing Interest

The authors declare that they have no known competing financial interests or personal relationships that could have appeared to influence the work reported in this paper.

## References

Alekseev, K.A., Mukhametzhanova, A.G., D'yakonov, G.S., 2017. Experimental investigations of velocity fields in packed bed

- static mixers. *Theor. Found. Chem. Eng.* 51 (3), 266–273. <https://doi.org/10.1134/S0040579517030010>
- Alberini, F., Bezchi, D., Mannino, I.C., Paglianti, A., Montante, G., 2021. Towards real time monitoring of reacting species and pH coupling electrical resistance tomography and machine learning methodologies. *Chem. Eng. Res. Des.* 168, 369–382. <https://doi.org/10.1016/j.cherd.2021.02.024>
- Alberini, F., Simmons, M.J.H., Ingram, A., Stitt, E.H., 2014. Use of an areal distribution of mixing intensity to describe blending of non-Newtonian fluids in a Kenics KM static mixer using PLIF. *AIChE J.* 60, 332–342. <https://doi.org/10.1002/aic.14237>
- Barkan-Öztürk, H., Delorme, J., Menner, A., Bismarck, A., 2022. Liquid-liquid extraction using combined hydrophilic-hydrophobic emulsion templated macro-porous polymer micro-mixer-settlers. *Chem. Eng. Process. - Process. Intensif.* 181, 109153. <https://doi.org/10.1016/j.cep.2022.109153>
- Baronti, L., Castellani, M., Hefft, D., Alberini, F., 2022. Neural network identification of water pipe blockage from smart embedded passive acoustic measurements. *Can. J. Chem. Eng.* 100, 521–539. <https://doi.org/10.1002/cjce.24202>
- Brunazzi, E., Paglianti, A., 1997. Mechanistic pressure drop model for columns containing structured packings. *AIChE J.* 43 (2), 317–327. <https://doi.org/10.1002/aic.690430205>
- Dimian, A.C., Bildea, C.S., Kiss, A.A., 2014. Process Intensification. In: *Computer Aided Chemical Engineering*. Elsevier B.V, pp. 397–448. <https://doi.org/10.1016/B978-0-444-62700-1.00010-3>
- Etchells, A.W., Meyer, C.F., 2004. Mixing in pipelines. In: Paul, E.L., Atiemo-Obeng, V.A., Kresta, S.M. (Eds.), *Handbook of Industrial Mixing*. Wiley-Interscience, Hoboken, USA.
- Forte, G., Albano, A., Simmons, M.J.H., Stitt, H.E., Brunazzi, E., Alberini, F., 2019b. Assessing Blending of Non-Newtonian Fluids in Static Mixers by Planar Laser-Induced Fluorescence and Electrical Resistance Tomography. *Chem. Eng. Technol.* 42, 1602–1610. <https://doi.org/10.1002/ceat.201800728>
- Forte, G., Brunazzi, E., Alberini, F., 2019a. Effect of residence time and energy dissipation on drop size distribution for the dispersion of oil in water using KMS and SMX+ static mixer. *Chem. Eng. Res. Des.* 148, 417–428. <https://doi.org/10.1016/j.cherd.2019.06.021>
- Ghanem, A., Lemenand, T., della Valle, D., Peerhossaini, H., 2014. Static mixers: Mechanisms, applications, and characterization methods - A review. *Chem. Eng. Res. Des.* 92, 205–228. <https://doi.org/10.1016/j.cherd.2013.07.013>
- Göbel, F., Golshan, S., Norouzi, H.R., Zarghami, R., Mostoufi, N., 2019. Simulation of granular mixing in a static mixer by the discrete element method. *Powder Technol.* 346, 171–179. <https://doi.org/10.1016/j.powtec.2019.02.014>
- Haddadi, M.M., Hosseini, S.H., Rashtchian, D., Ahmadi, G., 2020. CFD modeling of immiscible liquids turbulent dispersion in Kenics static mixers: Focusing on droplet behaviour. *Chin. J. Chem. Eng.* 28 (2), 348–361. <https://doi.org/10.1016/j.cjche.2019.07.020>
- Hosni, M., Hammoudi, M., Si-Ahmed, E., Legrand, J., Douib, L., 2022. Single and two-phase flows in a horizontal pipe with a Kenics static mixer: Effect of pressure drop on mixing. *Can. J. Chem. Eng.* <https://doi.org/10.1002/cjce.24402>
- Hou, R., Martin, P.J., Uppal, H.J., Kowalski, A.J., 2016. An investigation on using electrical resistance tomography (ERT) to monitor the removal of a non-Newtonian soil by water from a cleaning-in-place (CIP) circuit containing different pipe geometries. *Chem. Eng. Res. Des.* 111, 332–341. <https://doi.org/10.1016/j.cherd.2016.05.027>
- Jegatheeswaran, S., Ein-Mozaffari, F., Wu, J., 2018. Process intensification in a chaotic SMX static mixer to achieve an energy-efficient mixing operation of non-newtonian fluids. *Chem. Eng. Process.: Process. Intensif.* 124, 1–10. <https://doi.org/10.1016/j.cep.2017.11.018>
- Jiang, X., Xiao, Z., Jiang, J., Yang, X., Wang, R., 2021. Effect of element thickness on the pressure drop in the Kenics static mixer. *Chem. Eng. J.* 424, 130399. <https://doi.org/10.1016/j.cej.2021.130399>
- Kumar, V., Shirke, V., Nigam, K.D.P., 2008. Performance of Kenics static mixer over a wide range of Reynolds number. *Chem. Eng. J.* 139, 284–295. <https://doi.org/10.1016/j.cej.2007.07.101>

- Li, S., 2017. Residence time distribution and flow models for reactors. In: *Chemical Reaction Engineering*. Elsevier, pp. 213–263. <https://doi.org/10.1016/b978-0-12-410416-7.00005-7>
- Mahammedi, A., Ameer, H., Ariss, A., 2017. Numerical investigation of the performance of Kenics static mixers for the agitation of shear thinning fluids. *Open Access J. Appl. Fluid Mech.* 10 (3), 989–999 <https://doi.org/10.18869/ACADPUB.JAFM.73.240.27314>.
- Maluta, F., Montante, G., Paglianti, A., 2020. Analysis of immiscible liquid-liquid mixing in stirred tanks by Electrical Resistance Tomography. *Chem. Eng. Sci.* 227, 115898. <https://doi.org/10.1016/j.ces.2020.115898>
- Murasiewicz, H., Zakrzewska, B., 2019. Large Eddy Simulation of turbulent flow and heat transfer in a Kenics static mixer. *Chemical and Process Engineering. Inz. Chem. i Proces.* 40 (1), 87–99. <https://doi.org/10.24425/cpe.2019.126103>
- Murasiewicz, H., Jaworski, Z., 2013. Investigation of turbulent flow field in a Kenics static mixer by Laser Doppler Anemometry. *Chem. Pap.* 67 (9), 1188–1200. <https://doi.org/10.2478/s11696-013-0375-z>
- Nyande, B.W., Thomas, K.M., Takarianto, A.A., Lakerveld, R., 2022. Control of crystal size distribution in batch protein crystallization by integrating a gapped Kenics static mixer to flexibly produce seed crystals. *Chem. Eng. Sci.* 263, 118085. <https://doi.org/10.1016/j.ces.2022.118085>
- Paglianti, A., Montante, G., 2020. Simultaneous measurements of liquid velocity and tracer concentration in a continuous flow stirred tank. *Chem. Eng. Sci.* 216, 115495. <https://doi.org/10.1016/j.ces.2020.115495>
- Paglianti, A., Montante, G., 2013. A mechanistic model for pressure drops in corrugated plates static mixers. *Chem. Eng. Sci.* 97, 376–384. <https://doi.org/10.1016/j.ces.2013.04.042>
- Pahl, M.H., Muschelknautz E., 1982, Static mixers and their applications *International chemical engineering* 22 (2), 197–205.
- Poumaère, N., Pier, B., Raynal, F., 2022. Residence time distributions for in-line chaotic mixers. *Phys. Rev. E* 106, 015107. <https://doi.org/10.1103/PhysRevE.106.015107>
- Ramsay, J., Simmons, M.J.H., Ingram, A., Stitt, E.H., 2016. Mixing performance of viscoelastic fluids in a Kenics KM in-line static mixer. *Chem. Eng. Res. Des.* 115, 310–324. <https://doi.org/10.1016/j.cherd.2016.07.020>
- Rohkohl, E., Schönemann, M., Bodrov, Y., Herrmann, C., 2022. A data mining approach for continuous battery cell manufacturing processes from development towards production. *Adv. Ind. Manuf. Eng.* 4, 100078. <https://doi.org/10.1016/j.aime.2022.100078>
- Scala, M., Gamet, L., Malbec, L.-M., Li, H.-Z., 2020. Hydrodynamics of gas-liquid dispersion in transparent Sulzer static mixers SMXTM. *Chem. Eng. Sci.* 213 (art. no. 115398). <https://doi.org/10.1016/j.ces.2019.115398>
- Streiff, F.A., 1979, Adapted motionless mixer design. In: *Third European Conference on Mixing*, York, U.K., April 4–6th, 171–188.
- Streiff, F.A., Jaffer, S., Schneider, G., 1999, The design and application of static mixer technology. In: *Third International Symposium on Mixing in Industrial Processes*. Osaka, Japan, September 19–22th, 107–114.
- Thakur, R.K., Vial, C., Nigam, K.D.P., Nauman, E.B., Djelveh, G., 2003. Static mixers in the process industries - a review. *Chem. Eng. Res. Des.* 81 (7), 787–826. <https://doi.org/10.1205/026387603322302968>
- Theron, F., Sauze, N.L., 2011. Comparison between three static mixers for emulsification in turbulent flow. *Int. J. Multiph. Flow.* 37, 488–500. <https://doi.org/10.1016/j.ijmultiphaseflow.2011.01.004>
- Valdés, J.P., Kahouadji, L., Matar, O.K., 2022. Current advances in liquid-liquid mixing in static mixers: A review. *Chem. Eng. Res. Des.* 177, 694–731. <https://doi.org/10.1016/j.cherd.2021.11.016>
- Van Wageningen, W.F.C., Kandhai, D., Mudde, R.F., Van Den Akker, H.E.A., 2004. Dynamic flow in a kenics static mixer: An assessment of various CFD methods. *AIChE J.* 50 (8), 1684–1696. <https://doi.org/10.1002/aic.10178>
- Voulgaropoulos, V., Angeli, P., 2017. Optical measurements in evolving dispersed pipe flows. *Exp. Fluids* 58 (12), 170. <https://doi.org/10.1007/s00348-017-2445-4>
- Yao, Z., Alberini, F., Montante, G., Paglianti, A., 2023. A New Approach to Evaluate 3D Flow Fields Using an Off-Axis 2D PIV System: Investigation of a Tubular Reactor Equipped with Kenics Static Mixers. *Exp. Tech.* <https://doi.org/10.1007/S40799-023-00631-7>
- Yoon, J.-H., Lee, S.-J., 2002. Direct comparison of 2D PIV and stereoscopic PIV measurements. *Meas. Sci. Technol.* 13 (10), 1631–1642. <https://doi.org/10.1088/0957-0233/13/10/317>
- Wang, M., 2002. Inverse solutions for electrical impedance tomography based on conjugate gradients methods. *Meas. Sci. Technol.* 13 (1), 101–117. <https://doi.org/10.1088/0957-0233/13/1/314>
- Wang, M., Mann, R., Dickin, F.J., Dyakowski, T., 1996. Large-scale electrical tomography sensing system to study mixing phenomena. *Proceedings IWISP '96*. Elsevier, pp. 647–650. <https://doi.org/10.1016/B978-044482587-2/50142-7>